THE ASTROPHYSICAL JOURNAL, 481:83–94, 1997 May 20
© 1997. The American Astronomical Society. All rights reserved. Printed in U.S.A.

MERGER RATE OF EQUAL-MASS SPHERICAL GALAXIES

JUNICHIRO MAKINO
Department of Information Science and Graphics, College of Arts and Sciences, University of Tokyo, 3-8-1 Komaba, Meguro-ku, Tokyo 153, Japan

AND

PIET HUT
Institute for Advanced Study, Princeton, NJ 08540
Received 1995 September 26; accepted 1996 December 11

ABSTRACT

We present cross sections and reaction rates for merging to occur during encounters of equal-mass spherical galaxies. As an application, we determine the rate of galaxy merging in clusters of galaxies. We present results for two types of Plummer models (a full and a truncated one), two King models, and the Hernquist model. Cross sections are determined on the basis of a large number (~ 500) of simulations of galaxy encounters, using the 10 Gigaflops GRAPE-3A special purpose computer. We characterize the overall merger rate of galaxies in a galaxy cluster by a single number, derived from our cross sections by an integration over galaxy encounter velocities in the limit of a constant density in velocity space. For small clusters, where the cluster velocity dispersion may not significantly exceed the internal velocity dispersion of the individual galaxies, this constant-density approximation may not be valid. For those cases, we present separate results, based on integrations of our cross sections over Maxwellian velocity distributions. Finally, tidal effects from the cluster potential, as well as from neighboring galaxies, may prevent a barely bound galaxy pair from spiraling in after their first encounter. We give a quantitative estimate of the resulting reduction in the actual merger rate that is due to these tidal interactions.

Subject headings: galaxies: clusters: general — galaxies: interactions — methods: numerical

1. INTRODUCTION

Detailed simulations of galaxy encounters have become increasingly sophisticated during the last 25 years, as a result of significant improvement both in computer hardware and in algorithms used (for a recent review, see Barnes & Hernquist 1992). Most of these simulations attempt to explain features of specific encounters, often in an attempt to reproduce particular observations of interacting galaxies or merger remnants. In contrast, encounters between simpler galaxy models in order to obtain more general statistical results have received less attention.

The present paper attempts to address this latter problem by limiting ourselves to simulations of equal-mass galaxy models of various types, in order to determine merger cross sections and reaction rates. Our results can be readily applied to study the evolution of galaxy clusters, if we use our models to represent dark matter halos around galaxies in the limit that these halos can be considered to be spherical. In practice, moderate deviations from halo sphericity will not greatly affect our results.

The merger probability in an encounter of two galaxies is enhanced significantly when the encounter takes place at relatively low speed. For a given cluster of galaxies, with a given population of specified galaxy halos, the net merger rate can be determined by an integration of the usual $n\sigma v$ factor (density $\times$ cross section $\times$ velocity) over a Maxwellian or lowered Maxwellian velocity distribution. This procedure is sketched qualitatively in Figure 1*b* and can be compared to that used in stellar evolution calculations (Fig. 1*a*) where nuclear reaction rates are determined from the encounters of individual nuclei in the cores of stars. In the latter case, cross sections rise quickly with increasing encounter speed, leaving a small window for effective encounters well into the high-energy tail of the Maxwellian distribution. Our case of galaxy mergers, in contrast, is dependent on low-speed encounters and is determined by a relatively small window at the low-energy end of the Maxwellian distribution.

Figure 1*b* suggests that we can make a good start by representing the velocity distribution of the galaxies in the cluster as having a constant density in velocity space, i.e., $f(v) \propto v^2$ in three dimensions. This constant density can be obtained, for any given Maxwellian distribution, as the density of galaxies around the peak of the folded merger occurrence $f\sigma v$ in Figure 1*b*. In § 2 we describe some technical details of our calculations. In § 3 we present the cross sections, from which we determine reaction rates in § 4. In § 5, we determine the corrections to the reaction rates that are due to tidal effects. As an application, we present the rate of galaxy merging in clusters of galaxies in § 6, and we compare that with results from previous papers. Section 7 summarizes our results.

2. SIMULATIONS

2.1. *Units*

We choose our physical units of mass, length, and time by requiring that $M = r_v = G = 1$, where M is the mass of a single galaxy, r_v is the virial radius of a galaxy, and G is the gravitational constant (Heggie & Mathieu 1986). The virial radius is a measure of the size of a galaxy, defined so as to be able to express the potential energy of the galaxy to be equal to

$$E_{\rm pot} = -\frac{GM^2}{2r_v} . \tag{1}$$

In practice, the virial radius is not very different from the half-mass radius r_h. Typically,

$$r_h \simeq 0.8 r_v , \tag{2}$$

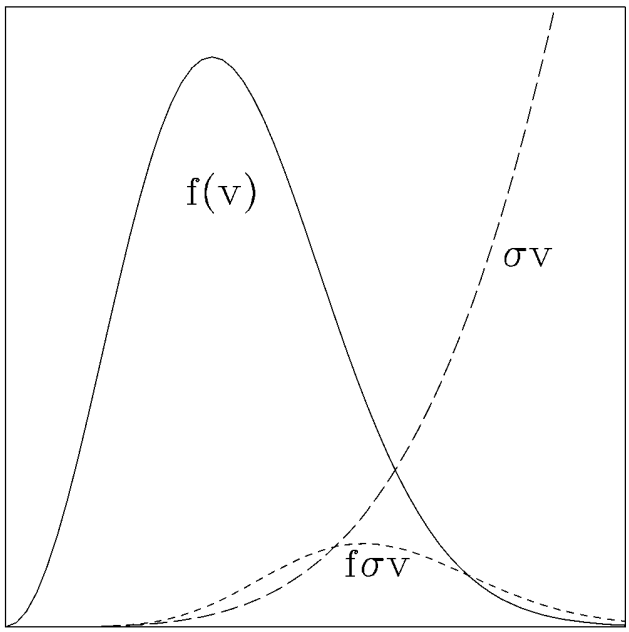

FIG. 1a

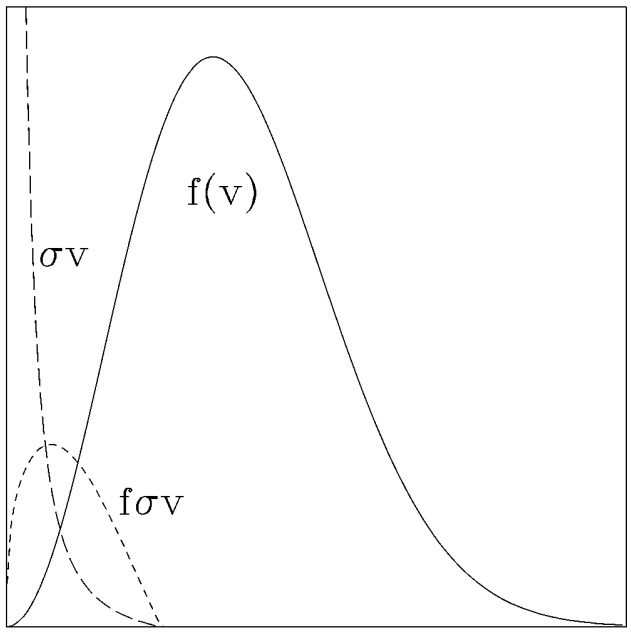

FIG. 1b

FIG. 1.—(*a*) Nuclear reaction rates in the core of a star, as the product of cross section σ and the rate factor $vf(v)$, with v denoting the relative velocities of the nuclei and $f(v)$ their Maxwellian distribution. (*b*) Merger rates in a rich cluster of galaxies, similar to the stellar evolution case.

with a coefficient generally in the range 0.76–0.98 (Spitzer 1987, § 1.2a). In our standard case of a Plummer model we have

$$r_h = \frac{3\pi}{16\sqrt{2^{2/3}-1}}\, r_v = 0.77 r_v \,, \tag{3}$$

for the Hernquist model

$$r_h = \frac{(1+\sqrt{2})}{3}\, r_v \,, \tag{4}$$

and for a constant-density sphere

$$r_h = \frac{3\times 2^{2/3}}{5}\, r_v = 0.95 r_v \,. \tag{5}$$

The main reason to take the virial radius, rather than the more usual half-mass radius, as our choice of units is a physical one: when we vary the internal structure of our galaxies, it is more meaningful to keep the total energy E of a galaxy constant than its half-mass radius. In our units,

$$E = E_{\rm pot}/2 = -\tfrac{1}{4} \,. \tag{6}$$

In terms of the particle positions, the virial radius is the harmonic mean particle separation

$$r_v = \left\langle \frac{1}{r_i - r_j} \right\rangle^{-1} \,, \tag{7}$$

averaged over all particle pairs $i \neq j$.

2.2. *Galaxy Models and Initial Conditions*

For the initial spherical galaxy model, we adopted five different choices: two Plummer models with different cutoff radii r_c (22.8 and 4), two King models with different values for the central potential W_c (1 and 7), and a Hernquist model (Hernquist 1990) with $r_c = 20$. We will indicate the Plummer model with $r_c = 4$ by "truncated Plummer" and the Plummer model with $r_c = 22.8$ simply by "Plummer."

These models provide a wide range of central condensation and halo distribution. They all have an isotropic velocity distribution since, according to Aguilar & White (1985), the difference in the velocity distribution is less important in determining merger cross sections than the difference in the density distribution. For all calculations, initial galaxies are modeled by 2048 equal-mass particles (except for several test calculations; see § 3.4). Thus the total number of particles per run is 4096. For Plummer models and King models, we constructed random realizations using an algorithm similar to the one described in Aarseth, Hénon, & Wielen (1974). For Hernquist models, we adopted a kind of "quiet start," in which particle i is initially placed in an arbitrary position on a sphere with a radius corresponding to the Lagrangian mass $(i - 0.5)/N$. The velocity of each particle was then chosen randomly from the velocity distribution function at that radius.

Since the initial galaxy models are spherical, the relative orbit of the two given galaxies is determined by only two parameters specifying the incoming branch of the hyperbolic Kepler orbit, the impact parameter ρ, and the relative velocity at infinity v. In this study, we found it more convenient to specify the initial orbit by v and the pericenter distance r_p of the extrapolated unperturbed hyperbolic orbit, in the limit that two galaxies would have been point masses. The reason to use r_p rather than ρ is related to the measurements of energy change during relatively wide encounters: keeping r_p constant allows us to let v smoothly go to zero in the parabolic limit, where $\rho \to \infty$.

Figure 2 shows the initial conditions used to determine the merging criterion for each models. The number of runs

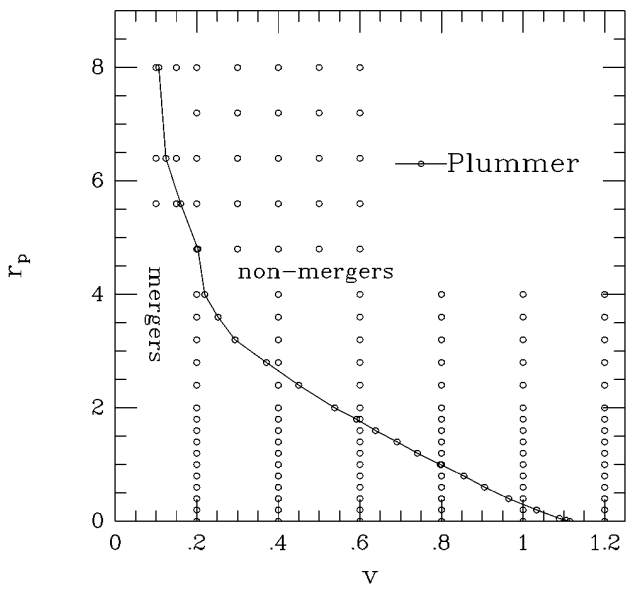

FIG. 2.—For each value of the pericenter distance r_p, circles indicate the choice of asymptotic velocities v for which a galaxy encounter has been carried out. Through linear interpolation of the energy dissipation, the critical velocity $v(r_p)$ for producing parabolic outgoing orbits is found for each r_p value. The full line connecting these points indicates the border of the region within which merger takes place.

for one model is 60–140. The following values for r_p were used: 0, 0.0125, 0.05, 0.2, 0.4, 0.6, 0.8, 1.2, 1.4, 1.6, 1.8, 2.0, 2.4, 2.8, 3.2, 3.6, 4.0, 4.8, 5.6, 6.4, and 8.0. For the initial separation between the two approaching galaxies, we choose a value of roughly 10 max (r_p, $2r_h$), where r_h is the half-mass radius of each of the two identical galaxies.

2.3. *Hardware and Numerical Integration Method*

We have used a GRAPE-3A (Okumura et al. 1993), a special purpose computer for collisionless N-body simulation, for all simulations. The GRAPE-3A performs the calculation of the gravitational interaction between particles. It is used with a host computer which is a UNIX-based workstation. All calculations except for the force calculation are performed on the host computer. One GRAPE-3A board hosts eight custom LSI chips, each of which calculates the gravitational interaction between particles in the speed of about 0.75 Gflops. Thus the peak speed of one board is 6 Gflops. For most runs, we have used two GRAPE-3A boards in parallel.

For the force calculation, we have used a simple direct-summation algorithm. Although it is perfectly possible to use the $O(N \log N)$ tree algorithm on the GRAPE systems (Makino 1991), it is not practical to do so for small particle numbers. The minimum number of particles for which the tree code is faster than the direct summation algorithm is $1–4 \times 10^4$, depending on the speed of the host computer. Since we typically used only 4096 particles, direct summation was much faster than the tree code.

We used the time-centered leap-frog integrator. The time step was 1/128 for all runs. The size of the softening parameter was $\epsilon = 1/32$. These parameters gave sufficient accuracy, resulting in a relative energy error well below 0.1% at the end of each calculation.

2.4. *Simulation Termination Procedure and Data Reduction*

For each choice of galaxy model and for each choice of pericenter distance r_p, we have carried out a series of galaxy encounter simulations at different values for the encounter velocity v (measured at infinity). For each of these simulations, we determine the energy of the relative orbit of the two galaxies, well after the first encounter, using the simple energy criterion:

$$E = -\frac{GM_1M_2}{r} + \frac{1}{2}\mu v^2 , \tag{8}$$

where M_1 and M_2 are the masses of two galaxies, r is the distance between two galaxies, G is the gravitational constant, and $\mu = M_1M_2/(M_1 + M_2)$ is the reduced mass, v is the relative velocity.

In Figure 3, we plot the energy $E(t)$ as a function of time t, for the case of Hernquist model initial conditions, with $r_p = 0.0125$ and $v = 1.2$. It is clear that the asymptotic value of the energy is reached soon after the encounter. However, to be on the safe side, we have extended all runs to reach a final separation comparable to the initial separation, where possible (for a bound final state, we have taken the minimum of this separation and the apocenter of the elliptic orbit). In this particular example, it takes far more time to reach the initial separation again because the outgoing orbit has far less positive energy and therefore the galaxies recede more slowly than they came in.

Having determined the asymptotic energy values $E(r_p, v)$, we select the pair of v-values between which the energy changes sign. We then use linear interpolation to determine the critical point $r_p(v)$ at which the outgoing orbit would have been just parabolic, separating the regions of merging and escape. Figure 2 indicates this process, for the case of Plummer models. Each circle represents a galaxy encounter run, and the full line connects the critical $r_p(v)$ points.

Figure 4 shows the same results, but translated from r_p values to ρ values. The impact parameter ρ is related to the pericenter distance r_p through the gravitational focusing relation (see eq. 14 below).

As a technical note, here is a brief description of the actual implementation of the energy determination,

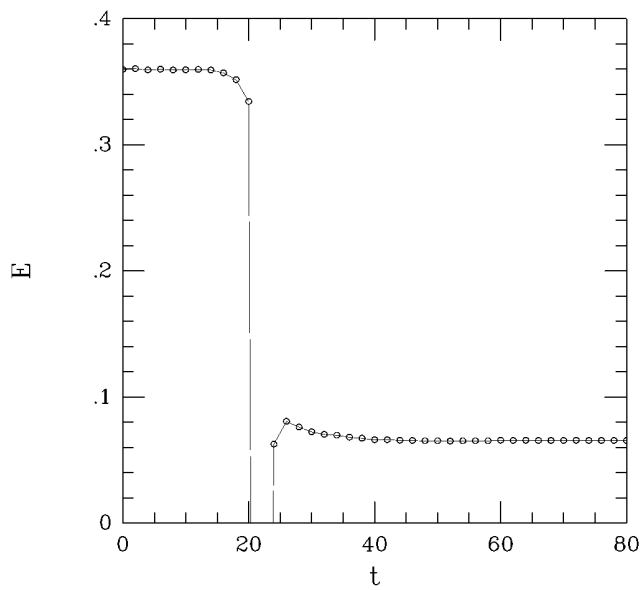

FIG. 3.—Total energy $E(t)$ of the two galaxies after the first encounter, as a function of time t, as specified in eq. (7). The initial lowering of the total energy is caused by the fact that the tidal interaction terms have been neglected in the calculation of the potential.

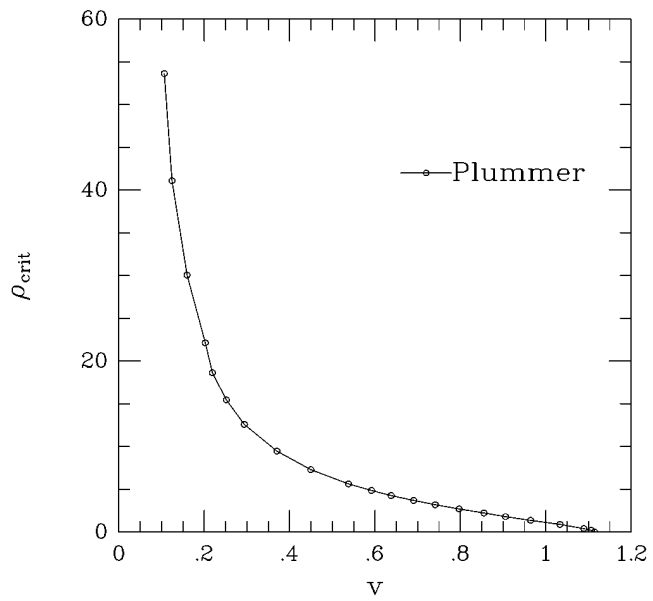

FIG. 4a

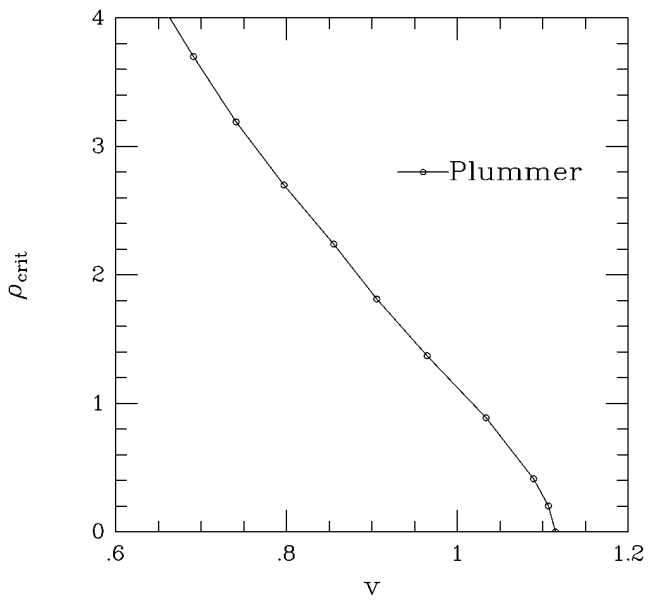

FIG. 4b

FIG. 4.—Maximum impact parameter $\rho_{crit}(v)$ for which merging takes place, as a function of velocity at infinity v, for Plummer model initial conditions. (*b*) An enlargement of (*a*), for small impact parameter values.

equation (8), in which appear the mass, position, and velocity of the galaxies after the encounter. They are calculated by the following procedure:

1. We make a crude guess for the center of mass of each galaxy. Here we use the center of mass of particles that are initially in one galaxy as the guess for the center of mass of the galaxy at that time.
2. For each particle, we determine to which galaxy it belongs. We calculate estimated binding energy given by

$$E_{ij} = -\frac{GM_j}{(r_{ij}^2 + R_0^2)^{1/2}} + \frac{1}{2} v_{ij}^2 , \qquad (9)$$

where r_{ij} is the distance between particle i and the estimated center of mass of the galaxy j, v_{ij} is the relative velocity between them, and R_0 is the length-scale parameter that represents the depth of the potential well of galaxies. We use $R_0 = 0.6$, which gives a fairly accurate estimate for the potential for Plummer models. We then make our initial guess as to which galaxy particle i mostly likely might be bound by assigning it to galaxy 1 if $E_{i1} < E_{i2}$ or to galaxy 2 if $E_{i1} > E_{i2}$.
3. For each galaxy, we determine which of the particles that are labeled as belonging to it are actually bound to the galaxy. If the binding energy of a particle relative to the galaxy is positive, we regard it as an unbounded escaper.
4. We repeat step (3) until membership converges.

Most of the data reduction was performed using the NEMO software package, in the version provided by Teuben (1995).

3. CROSS SECTIONS FOR GALAXY MERGING

3.1. *Results and Scaling Relations*

Figure 5 shows the critical velocity for merging v_{crit} as a function of the impact parameter ρ for all galaxy models used. The merging criterion determined experimentally here shows only a weak dependence on the galaxy model: for the whole range of impact parameters studied, the difference in v_{crit} among the different models is less than 20%. For the Plummer model, we find a good fit with $v_{crit} \propto \rho^{-0.75}$ for large ρ, as plotted for comparison in Figure 5. For the King model with $W_c = 1$ the index is slightly larger and for $W_c = 7$ the index is slightly smaller. The slope for the Hernquist model is somewhat smaller still.

At first sight, these results seem to be in good agreement with the distant tidal impulsive approximation, which indeed predicts a relationship $v_{crit} \propto \rho^{-0.75}$ for large ρ. The tidal impulsive approximation has been used by many researchers to obtain analytic approximations for changes

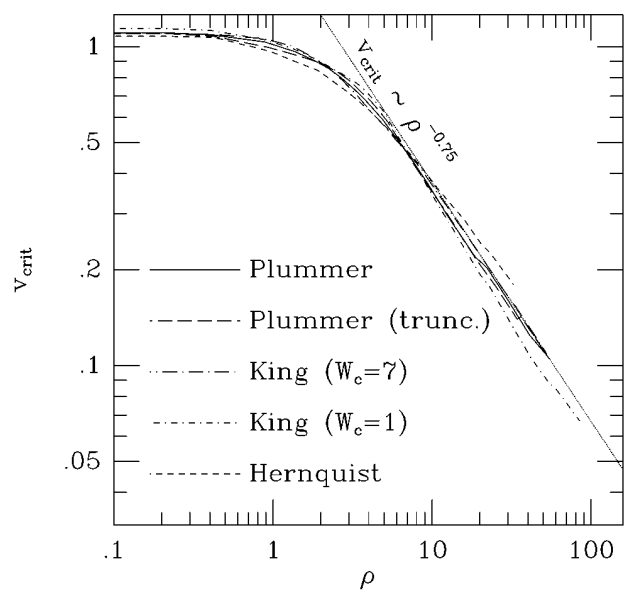

FIG. 5.—Maximum velocity $v_{crit}(\rho)$ for which merger takes place. The impact parameter ρ and v_{crit} are both asymptotic values, in the limit of infinite initial galaxy separation. Solid, short-dashed, long-dashed, short–dot-dashed and long–dot-dashed curves are results for Plummer (r_{cut} = 23), King ($W_c = 1$), King ($W_c = 7$), Plummer ($r_{cut} = 4$), and Hernquist models, respectively.

in mass and energy of galaxies involved in relatively weak encounters (Richstone 1975; White 1979; Dekel, Lecar, & Shaham 1980; Richstone & Malumuth 1983). In this approximation, the loss of energy of the relative orbital motion of the two galaxies scales as

$$\Delta E \propto \left(\frac{GM}{r_p^2 v_p}\right)^2 , \tag{10}$$

where r_p and v_p are the relative distance and relative velocity at closest approach. For the critical velocity, the energy loss is equal to the kinetic energy of the orbital motion at infinity,

$$\Delta E = \tfrac{1}{2}\,\mu v^2 , \tag{11}$$

where $\mu = M/2$ is the reduced mass. If we apply the point mass approximation for the relative orbit, the relations between the orbital elements are given by conservation of angular momentum and energy as

$$\rho v = r_p v_p ,$$

$$\frac{1}{2}\,\mu v^2 = \frac{1}{2}\,\mu v_p^2 - \frac{GM^2}{r_p} . \tag{12}$$

Here we assume that $\mu v^2 \ll GM^2/r_p$. Under this assumption, the last equality is reduced to

$$v_p = \sqrt{\frac{4GM}{r_p}} . \tag{13}$$

The resulting pericenter distance is then given as

$$r_p = \frac{\rho^2 v^2}{4GM} , \tag{14}$$

and the incoming velocity can now be expressed in terms of the impact parameter as

$$v \propto \rho^{-3/4} , \tag{15}$$

seemingly in good agreement with the data shown in Figure 6.

3.2. *The Masking Tendency of Gravitational Focusing*

This good agreement is, however, fortuitous and does not reflect the physical reality. The discrepancies can be seen clearly in Figure 6, which shows the critical velocity v_m as a function of pericenter distance r_p. If the tidal approximation were really valid, the results for all models would show the same asymptotic behavior of $v \propto r_p^{-3/2}$. The results for the Plummer models and the concentrated King model is close to the theoretical line. However, the results for the Hernquist model and the shallow King model deviate significantly.

Indeed, there was no reason to expect an impulsive tidal approximation to give us guidance in estimating the critical velocity for mergers to take place. As is clear from Figure 6, mergers at large r_p take place for nearly parabolic orbits, where the duration of relatively close encounters around pericenter passage is drawn out to a total time exceeding that of the half-mass crossing time. There is no reason to expect, under these circumstances, that any type of impulsive approximation would be valid.

Why, then, did Figure 5 show such a good correspondence with the line $v_{\rm crit} \propto \rho^{-0.75}$? The reason can be found in a conspiracy of gravitational focusing effects together with the real merger criterion. This can be seen as follows.

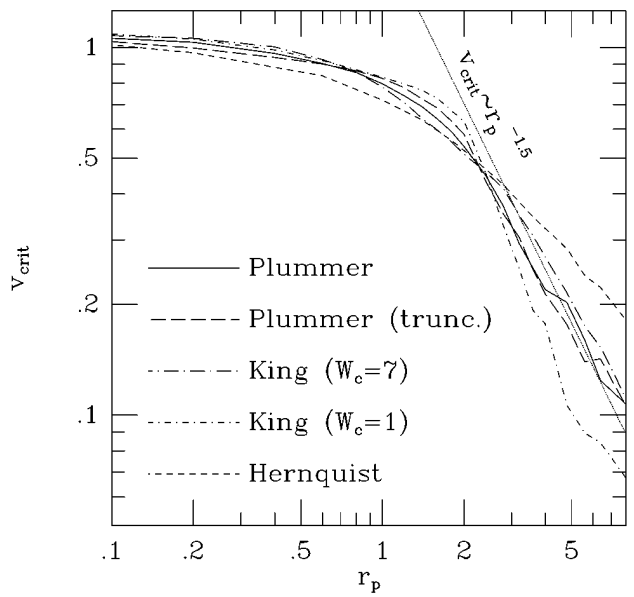

FIG. 6.—As Fig. 5, but with the merger velocity $v_{\rm crit}(r_p)$ now plotted against the pericenter distance r_p. The tidally impulsive limit, the line $v_{\rm crit} \propto r_p^{-3/2}$, is given here for comparison.

Suppose that we start with a relation for the energy loss in the form of a power law

$$\Delta E \propto r_p^{-\alpha} . \tag{16}$$

For the critical velocity at infinity, we then have

$$v \propto r_p^{-\alpha/2} . \tag{17}$$

From equation (14), we obtain

$$v \propto \rho^{-\alpha/(\alpha+1)} . \tag{18}$$

The slope of this relation between ρ and v lies in the range $\{-1, 0\}$, for *any* positive value of α. This implies that even large differences in the relations between nearest approach and energy loss are not very well visible in Figure 5.

From a practical point of view, this reasoning has an interesting consequence: equation (18) implies that the merging cross section is relatively insensitive to the fact that the amount of energy loss varies widely among different models when measured at the same pericenter distance.

From a theoretical point of view, we already saw that the impulsive tidal approximation is not reasonable. More specifically, the timescale of the encounter is proportional to $r_p^{1.5}$. If this encounter timescale significantly exceeds the orbital timescale of a particle in the galaxy, the binding energy of that particle becomes an adiabatic invariant. As a result, the energy change decays exponentially as a function of increasing r_p. If a galaxy has a finite radius r, encounters with $r_p \gg r$ will result in only a very small energy change, and $v(r_p)$ would thus decrease exponentially.

3.3. *Theoretical Scaling Arguments*

A simple alternative to the impulsive approach could start with a determination of the amount of significant particle overlap during the encounter. A quick inspection of Figures 5 and 6 already shows that this may be a reasonable approach, when we realize the exceptional nature of the Hernquist & King ($W_c = 1$) models. These are the two models that deviate most in both figures, and, indeed, these

are the two models that deviate most in the position of the radius that encloses 95% of the mass in each model, with the King ($W_c = 1$) model having an unusually sharp cutoff and the Hernquist model having an unusually large amount of matter far from the core region (see also Fig. 12).

If a galaxy has an extended halo with a power-law density profile, the particles in the region outside the radius r_p have orbital timescales comparable to, or longer than, the timescale of the encounter. As a result, those particles are strongly perturbed, and we can still expect the impulsive approximation to give a reasonable estimate, at least in order of magnitude. Thus the energy gain of particles outside the radius r_p can be estimated from the typical velocity kick Δv they receive as

$$\Delta E_{\rm out} \approx [M - M(r_p)](\Delta v)^2 = [M - M(r_p)]\left(\frac{2GM}{r_p v_p}\right)^2 , \quad (19)$$

where $M(r)$ is the mass of a single galaxy enclosed inside the radius r (the total mass $M = 1$ initially, in our units). The velocity v_p at pericenter passage is related to r_p in the parabolic approximation by $\frac{1}{2}v_p^2 \approx GM/r_p$. This gives

$$\Delta E_{\rm out} \approx \frac{G[M - M(r_p)]M}{r_p} . \quad (20)$$

Note that this energy change is equal to the binding energy of the mass outside the radius r_p. In other words, in our approximation all particles are divided into two groups, an inner and an outer group. The inner particles are considered to be left undisturbed, while the outer ones are significantly perturbed during the encounter.

For galaxy models with a halo described by a power-law density $\rho_d = r^{-\beta}$, we have $[M - M(r)] \propto r^{-\beta+3}$ and

$$\Delta E_{\rm out} \propto r_p^{2-\beta} , \quad v \propto r_p^{1-\beta/2} . \quad (21)$$

For the Hernquist model, $\beta = 4$. Therefore the power index in the latter relation is -1. For the Plummer model, $\beta = 5$, and the index becomes $-3/2$.

Figure 7 shows the critical velocity obtained by N-body simulations and that estimated using equation (20). For both Plummer and Hernquist models, the theoretical estimate and the numerical result show a reasonable agreement, well within a factor of 2 for r_p values in the range $\{1, 20\}$. This is a very satisfactory result, given the simple nature of our approximations.

3.4. *Cross Sections*

From the $\rho_m(v)$ results, plotted in Figures 4 and 5, it is straightforward to determine the cross section $\sigma(v)$ for mergers to occur:

$$\sigma(v) = \pi\rho^2 . \quad (22)$$

The results are plotted in Figure 8.

A more useful way to display these cross sections is by multiplying them by a factor v^3. The first two factors of v reflect the three-dimensional nature of a Maxwellian velocity distribution, with a velocity space volume factor of $v^2\,dv$ (see eq. [29]), while the third factor indicates the fact that, for a fixed target size, the rate of merging encounters is proportional to the relative velocity of the galaxies involved.

The results, in the form of $v^3\sigma(v)$, are plotted in Figure 9. There is a slight gap at the left-hand side of the curves, where it would have been too time-consuming to determine the critical merger velocities through numerical simulations. Fortunately, we can use the arguments developed in § 3.3 to extrapolate our numerical results leftward of where the curves end. For galaxy models with a halo described by a power-law density $\rho_d = r^{-\beta}$, we find from equations (14) and (21) that

$$\rho \propto v^{(\beta-1)/(2-\beta)} . \quad (23)$$

This leads directly to

$$\sigma v^3 \propto \rho^2 v^3 \propto v^{(\beta-4)/(\beta-2)} . \quad (24)$$

For a Hernquist model, with $\beta = 4$, we see that this quantity tends to a constant value for vanishing v, while for a

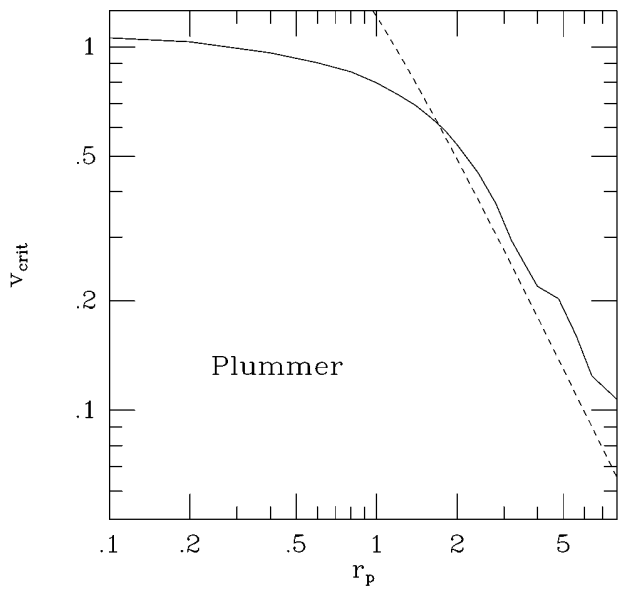

FIG. 7a

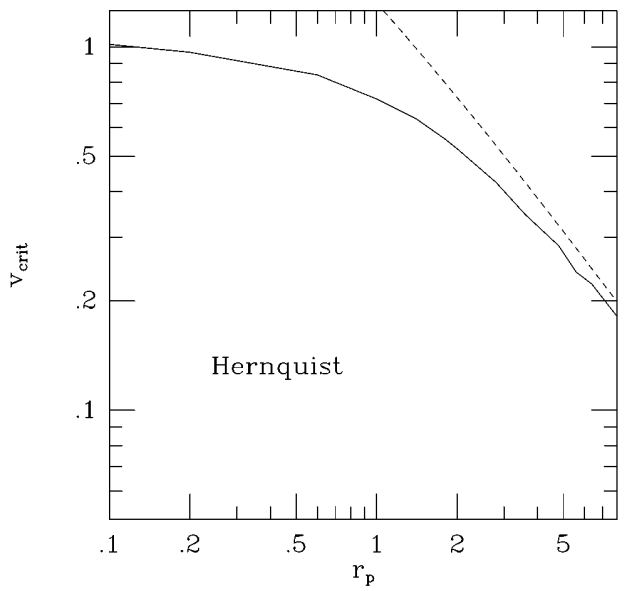

FIG. 7b

FIG. 7.—Same as Fig. 6, but including the theoretical estimate for large r_p. (*a*) Experimental results for a Plummer model, together with the theoretical estimate $v_{\rm crit} \propto r_p^{-3/2}$. (*b*) Similar results for a Hernquist model, together with the theoretical estimate $v_{\rm crit} \propto r_p^{-1}$.

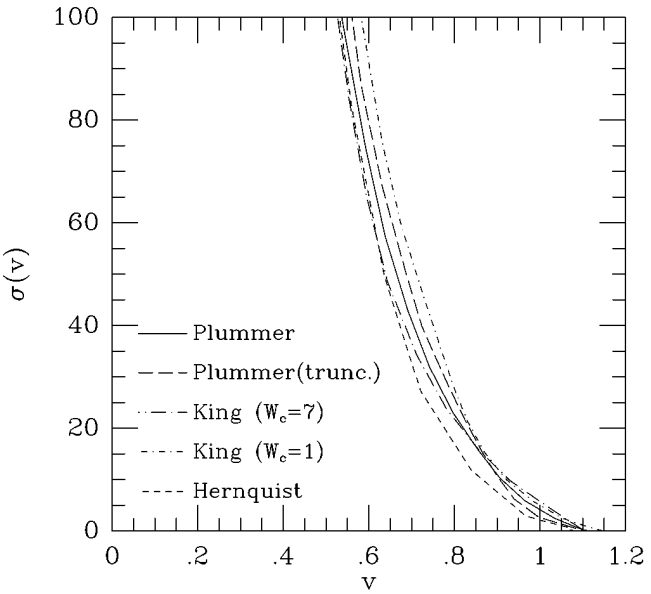

FIG. 8.—Merging cross section $\sigma(v)$, where v is the initial encounter velocity (at infinity). The various lines have the same meaning as those in Fig. 5.

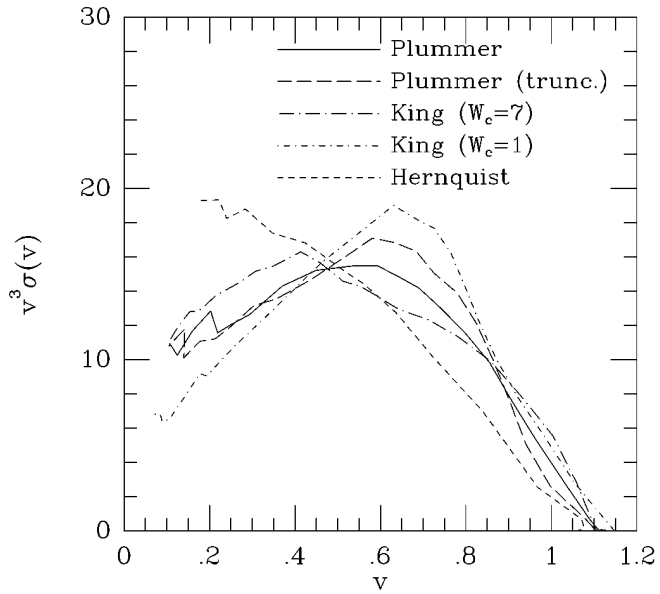

FIG. 9.—The differential merging rate $v^3\sigma(v)$ plotted as a function of the velocity v for five different galaxy models. The curves have the same meanings as in Fig. 5.

Plummer model this quantity tends to scale as $v^{1/3}$ for low v values. In the rate determinations of § 4, we will use these analytic extrapolations to augment the numerical data.

3.5. *Error Discussion*

In our simulations, the total number of particles per galaxy has been typically $N = 2 \times 10^3$. Depending on the exact definition of half-mass relaxation time $t_{\rm hr}$ and half-mass crossing time $t_{\rm hc}$, we can get somewhat different relationships between these two quantities. Let us take as a reasonably accurate choice the expression $t_{\rm hr}/t_{\rm hc} = 0.1N/\ln(0.4N)$ (see Spitzer 1987 for the factor 0.4). For $N = 2 \times 10^3$, this gives us $t_{\rm hr}/t_{\rm hc} \simeq 30$. However, we have used a softening length of 1/32. With a strong-deflection distance of order $1/N$, the added softening increases the relaxation time by a factor $\log N/\log 32 \simeq 2$. Our galaxies can thus be expected to show significant relaxation after 60 half-mass crossing times. In our units, the internal three-dimensional velocity dispersion of a galaxy is $1/2^{1/2}$, and the time to cross the system, starting at the half-mass radius, is therefore $\sim 2/2^{1/2} \simeq 3$. Thus, we can expect significant relaxation to occur after ~ 200 time units.

For the simulation in Figure 3, relaxation effects are not expected to be very important, given a total duration of the simulation of 100 time units. However, for larger impact parameters, the duration of a typical encounter simulation can be significantly longer, and relaxation effects may begin to influence the measurements of energy dissipation. This in turn will effect the determination of the border line for mergers to take place at high values for the impact parameter.

We have run various tests in order to determine the systematic errors that can occur for large r_p values. For example, for the King models with $W_c = 1$, we have rerun a number of experiments, using a total particle number per galaxy in the range $512 \leq N \leq 16384$, as compared to our standard value $N = 2048$. For relatively small pericenter values, such as $r_p = 0.1$ and $r_p = 3.2$, we did not find any noticeable change for the final merger boundary value $v_m(r_p)$. In fact, even downgrading our runs by a factor of 4 in total particle number did not have a significant effect on the outcome.

However, for $r_p = 6.4$, we found that the measured $v_m(r_p)$ steadily decreased for increasing particle numbers, until leveling off for a value of N that is 4 times larger than originally used. As a consequence, the reduction in slope in the lower right corner in the line labeled "King" ($W_c = 1$) in Figure 6 is not correct. In the limit of $N \to \infty$, the line will continue to descend with a near-constant slope, leading to v_m values around $r_p = 8$ that are roughly half of what we have obtained here for our standard value of $N = 2048$ particles per galaxy. However, these systematic errors do not contribute significantly to the overall reaction rates, as we can see in Figure 9.

4. MERGER RATES

Given the cross section determined in the previous section, we are now in a position to determine the rate at which mergers occur, by averaging over a distribution of velocities.

The distribution function for the velocity of the galaxies inside a cluster is given in a Maxwellian approximation by

$$f_1(v) = \left(\frac{2}{\pi}\right)^{1/2} \sigma_e^{-3} v^2 e^{-v^2/2\sigma_e^2} , \tag{25}$$

where σ_e is the one-dimensional velocity dispersion for the cluster.

The distribution of encounter velocities is then given by

$$f_2(v) = 2^{-1}\pi^{-1/2}\sigma_e^{-3} v^2 e^{-v^2/4\sigma_e^2} , \tag{26}$$

where in both cases we use a normalization condition of unity after integration over velocities:

$$\int_0^\infty f_1(v)dv = \int_0^\infty f_2(v)dv = 1 . \tag{27}$$

Let us introduce the ratio x of the one-dimensional

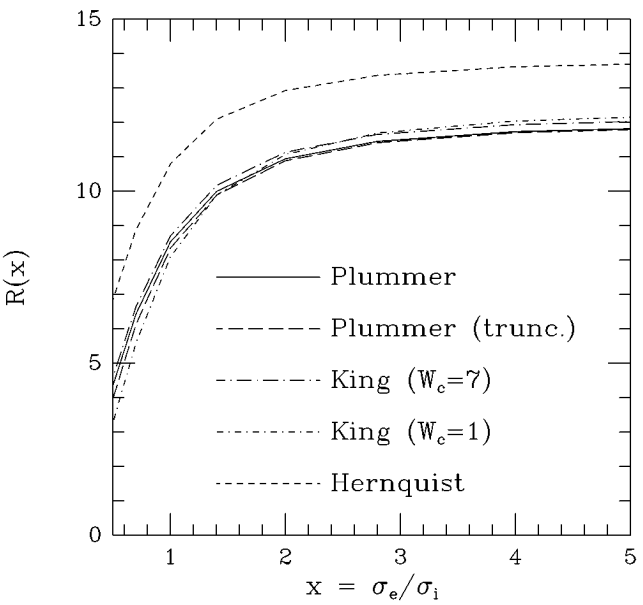

FIG. 10.—Merger rate $R(x)$ as a function of the ratio of velocity dispersions: σ_e indicates the velocity dispersion of the galaxies inside the galaxy cluster, and σ_i the internal velocity dispersion for the stars inside each galaxy model.

velocity dispersion of the cluster and the one-dimensional internal velocity distribution of the stars in each galaxy,

$$x = \frac{\sigma_e}{\sigma_i} = \sqrt{6}\sigma_e \,, \tag{28}$$

since $\sigma_i = 1/6^{1/2}$ in our units in which the specific kinetic energy $(3/2)\sigma_i^2 = 1/4$. We thus have

$$f_2(v) = 2^{-1}\pi^{-1/2}\sigma_e^{-3}v^2 e^{-3/2v^2/x^2} \,, \tag{29}$$

The number of merging events per unit time per unit volume is given by

$$R(n, x) = n^2 \int_{v=0}^{\infty} v f_2(v)\sigma(v)dv \,, \tag{30}$$

where n is the number density of the galaxies and $\sigma(v)$ is the cross section of merging.

We can also write this result as

$$R = n^2 2^{-1}\pi^{-1/2}\sigma_e^{-3}R(x) \,, \tag{31}$$

where $R(x)$ is the nondimensional merging rate defined as

$$R(x) = \int_0^{v_{\rm crit}} v^3\sigma(v)e^{-3/2v^2/x^2}\,dv \,, \tag{32}$$

where the upper limit of integration is reached at $v_{\rm crit}$ since the cross section $\sigma(v) = 0$ for $v > v_{\rm crit}$.

Note that in our units it is not immediately clear that this last expression is dimensionless. If we remind ourselves of the fact that our internal one-dimensional velocity dispersion $\sigma_i = 1/6^{1/2}$ and the virial radius of an individual galaxy $r_v = 1$, we can rewrite the expression for $R(n, x)$ as

$$R = n^2 2^{-1}\pi^{-1/2} r_v^2 \frac{(36\sigma_i^4)}{\sigma_e^3} R(x)$$

$$= \frac{18}{\sqrt{\pi}} \frac{1}{x^3} n^2 r_v^2 \sigma_i R(x) \,, \tag{33}$$

TABLE 1

NONDIMENSIONAL MERGER RATE

Model	R_∞
Plummer	11.9
Plummer ($r_{\rm cut} = 4$).....	11.5
King ($W_c = 1$)	12.4
King ($W_c = 7$)	11.8
Hernquist.....	13.8

from which it is clear that $R(x)$ is dimensionless since all physical factors (density squared × cross section × velocity) have been displayed here explicitly.

In rich clusters, the velocity dispersion σ_e in the cluster is several times larger than the internal velocity dispersion σ_i in each of the galaxies. Even for less rich clusters, $\sigma_e > \sigma_i$, typically.

Figure 10 shows $R(x)$. For $x \gtrsim 2$, R is close to the asymptotic value for $x \to \infty$. Thus, for most rich clusters, the merging rate calculated with constant $f(v)$ gives an error less than a few percent. For that regime, the dimensionless merging rate is given by

$$R_\infty = \lim_{x\to\infty} R(x) = \int_0^{v_{\rm crit}} v^3\sigma(v)dv \,. \tag{34}$$

Note that R_∞ does not depend on the velocity distribution of galaxies within the cluster. The only dependency on the external velocity dispersion σ_i is through the factor σ_e^{-3} in the expression for R itself. This is simply the dilution factor in velocity space: increasing the external velocity dispersion decreases the density of galaxies within the region in which encounters can lead to merging.

Table 1 shows the nondimensional merging rate R_∞ for all models. For nonzero values of x, we can approximate $R(x)$ for most models by the following fitting formula

$$R_{\rm P}(x) = \frac{12x^2}{x^2 + 0.42} \,, \tag{35}$$

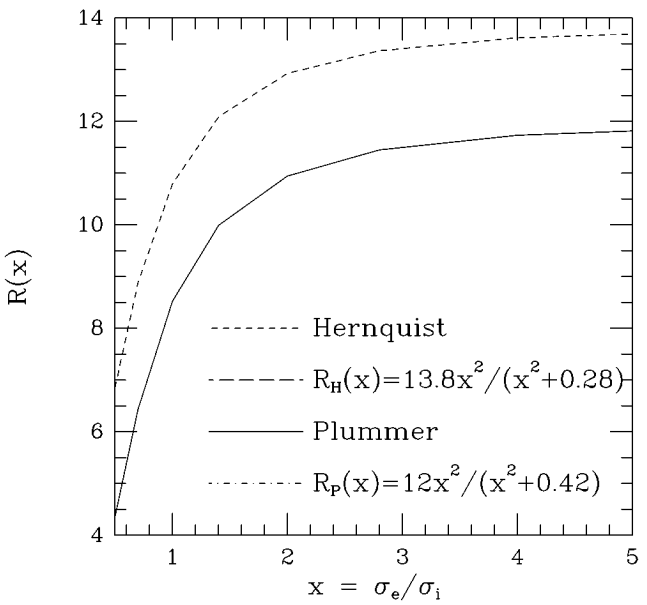

FIG. 11.—As Fig. 10, with the Plummer model and the Hernquist model, together with their respective fitting formulas $R_{\rm P}(x)$ and $R_{\rm H}(x)$, given in eqs. (34)–(35).

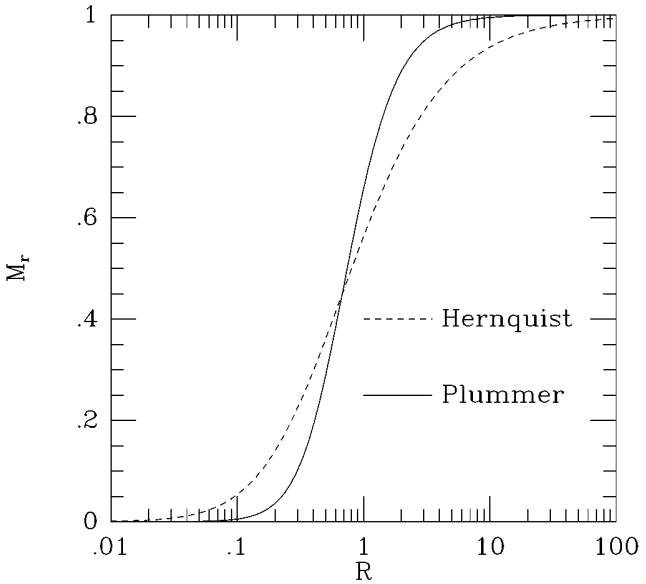

FIG. 12.—Cumulative mass is plotted here for the Plummer model and the Hernquist model. The more extended mass distribution of the latter is responsible for the higher merger rate of the Hernquist model in Figs. 10 and 11.

while for the Hernquist model a better approximation is given by the fitting formula

$$R_{\rm H}(x) = \frac{13.8x^2}{x^2 + 0.28} . \tag{36}$$

Figure 11 shows these fitting formulae and experimental results. The agreement is quite good. The physical reason behind the fact that the Hernquist model shows a merging rate that is 15% larger than the Plummer model lies in the more extended mass distribution of the former, as is illustrated in Figure 12.

5. TIDAL EFFECTS

In our discussion of the merger cross section and the merger rate, we have so far regarded two galaxies as actually merging if the orbital binding energy of the two galaxies after the first encounter is negative. Simple and straightforward as this assumption is, it may not be realistic in some extreme cases, as for example in rich clusters. In such cases, even if two galaxies have become formally bound after their first encounter, they may still be disrupted under the influence of either the tidal forces from the cluster as a whole or the tidal forces from individual nearby galaxies. In the following, we evaluate the magnitude and relevance of both of these effects.

5.1. *Tidal Effects from the Cluster as a Whole*

Consider a cluster consisting of N galaxies. The tidal force from the cluster would dissolve a pair of galaxies if the separation of the pair is larger than $fR(ND)^{-1/3}$, where R is the radius of the cluster and D is the ratio of the total mass of the cluster to the mass associated with the individual galaxies. The coefficient in this expression would be $f = 1/3$ in the limit in which the cluster mass is all concentrated in the center (Spitzer 1987, eq. [5-5]). For more realistic mass distributions, the tidal force on a typical merging pair is considerably less, and therefore f is significantly larger. A reasonable approximation is therefore to simply take $f = 1$.

Thus, we discard a candidate merger pair if their first apocenter distance exceeds

$$r_{t,\rm global} = R(ND)^{-1/3} . \tag{37}$$

5.2. *Tidal Effects from Individual Nearby Galaxies*

To determine the tidal effects of neighboring galaxies acting as perturbers requires a somewhat more complicated calculation. For a pair of galaxies in the process of merging to become unbound by the encounter with a third galaxy, this latter galaxy should pass within a distance that is sufficiently close, during a time that is sufficiently quick, i.e. before the first fallback. Since most orbits after the first flyby are highly eccentric, the fallback time can be approximated by the orbital period itself, which is given for a pair of galaxies by

$$T = \pi\sqrt{\frac{2a^3}{m}} , \tag{38}$$

where a is the semimajor axis of the pair and m is the mass of one galaxy.

We can apply the usual $n\sigma v$ argument for the rate in order to determine a disruption criterion of the pair. For the pair to be disrupted, we have

$$n\sigma vT \geq 1 \tag{39}$$

as an approximate formula. Here we can estimate the density n to be of order

$$n = N/R^3 . \tag{40}$$

A typical relative velocity value is given by the virial theorem as

$$v \sim \sqrt{\frac{2DNm}{R}} . \tag{41}$$

We neglect gravitational focusing for the perturbers, which will fly by with a velocity much higher than the relative velocity of the two merger candidates around the apocenter of their first orbit. This means that we can use the geometrical cross section

$$\sigma = \pi r^2 . \tag{42}$$

We can make a quantitative estimate for this cross section as follows. The average amount of energy transferred by a third galaxy that passes at a distance r from one of the galaxies in the pair is given in the impulse approximation by

$$\Delta E \sim \frac{1}{2} m\left(\frac{m}{vr}\right)^2 . \tag{43}$$

This energy change must be larger than the binding energy of the pair $m^2/2a$. Thus, we obtain

$$r^2 \sim am/v^2 \tag{44}$$

as the maximum encounter distance to disrupt a pair.

We can find a second expression for this distance, using equation (39). Using both expressions to eliminate r and substituting v from equation (41), we find

$$a > (2/\pi^4)^{1/5} RN^{-1/5} D^{1/5} \tag{45}$$

as the condition for disruption. Taking into account that the first bound orbit, after the initial encounter, is likely to be highly eccentric, we can approximate the apocenter distance after the first encounter to be $r_{\rm apo} \simeq 2a$. The criterion

for tidal disruption from a single nearby galaxy then becomes $r_{\rm apo} > r_{t\ \rm local}$, with

$$r_{t,\rm local} = RN^{-1/5}D^{1/5} . \quad (46)$$

Comparing equations (37) and (46), we see that the latter critical distance exceeds the former by a factor

$$r_{t,\rm local}/r_{t,\rm global} = N^{2/15}D^{8/15} > 1 , \quad (47)$$

since $D \geq 1$ by definition. Typical values for this ratio will be ~ 10 for rich clusters.

In conclusion, we see that the tidal forces exerted by neighboring galaxies are less important than the tidal force exerted by the parent cluster as a whole, in its effectiveness to disrupt a galaxy pair while it has become bound after its first encounter.

How large is the critical distance $r_t = \min\ (r_{t,\rm local}, r_{t,\rm global}) = r_{t,\rm global}$ for tidal disruption in real clusters? For a cluster of N galaxies, and using the notion introduced in equation (28), we find that the half-mass radius of the cluster is larger than that of the individual galaxies by a factor of ND/x^2. Thus, using equation (37) we obtain

$$r_t = (ND)^{2/3}x^{-2}r_h , \quad (48)$$

for the maximum apocenter distance after the encounter at which tidal disruption can be avoided.

To sum up, tidal effects will disrupt those mergers that have a binding energy less than a critical value E_t, given by

$$E_t \sim \frac{M^2}{r_t} = \frac{-5x^2E}{(ND)^{2/3}} = \frac{5}{4}\frac{x^2}{(ND)^{2/3}} , \quad (49)$$

where we have used equation (2), with E the internal energy of one galaxy ($E = -\frac{1}{4}$ in our units; see eq. [6]).

For typical clusters, E_t lies in the range $0.01 \lesssim E_t \lesssim 0.1$. For example, for a cluster with $N = 100$, $D = 3$, and $x = 2$, we have $E_t \sim 0.1$, while for a rich cluster with $N = 1000$, $D = 10$, and $x = 3$, we have $E_t \sim 0.02$.

5.3. *Sensitivity of Cross Sections to Tidal Effects*

In order to calculate the cross section as a function of critical binding energy for tidal disruption E_t, we could perform a systematic search as we did for the case of $E_t = 0$. Since this would require rerunning many of our simulations separately for each value of E_t, it would be preferable to check whether an appropriate approximation exists that would allow us to derive a merging criterion for nonzero E_t to a reasonable accuracy.

The merging criterion is expressed as

$$E_1 = E_0 + \Delta E < E_t , \quad (50)$$

where E_0 and E_1 are the orbital binding energy of two galaxies before and after the first encounter, and ΔE is defined as $E_1 - E_0$. ΔE is a function of collision parameters ρ and v, or r_p and v_p, as described in § 3.

As an approximation, we assume that ΔE is determined essentially by r_p alone, at least when the relative velocity is close to the critical velocity for merging. Thus, we have, as a first approximation,

$$\Delta E = -\tfrac{1}{2}\mu v_{\rm crit}^2 , \quad (51)$$

and therefore

$$E_1 = \tfrac{1}{2}\mu(v^2 - v_{\rm crit}^2) . \quad (52)$$

It is reasonable to expect this assumption to be quite good for most cases since v_p is determined mainly by the potential energy at minimum separation and depends only weakly on v, the velocity at infinity.

To test whether this approximation is satisfactory, we compare the result of our numerical experiments and the theoretical estimate obtained by assuming that ΔE is independent of the velocity at infinity. Figure 13 shows the orbital energy of the relative motion of the two galaxies, in units of the kinetic energy associated with the critical velocity $v_{\rm crit}$,

$$\epsilon_{\rm orb} = \frac{2E_{\rm orb}}{\mu v_{\rm crit}^2} , \quad (53)$$

plotted against the initial orbital velocity at infinity, in units of the critical velocity. Note that $v_{\rm crit}$ is calculated for the pericenter distance r_p derived from the impact parameter ρ through the two-body Keplerian gravitational focusing approximation. The approximation of velocity-independent energy dissipation, given by equation (52), is given in Figure 13 by the solid curve.

The agreement between theory and experiment is excellent for a wide range of initial relative velocities. Therefore, in the following we will assume that ΔE is a function of r_p alone.

Figure 14 shows the effects of nonzero E_t in terms of the differential merger rate $v^3\sigma$. It is clear that the reduction in the merging probability is significant, especially for the Hernquist model. The reduction is largest for lower velocities, for which a typical binding energy of the orbit after the first encounter is lower, and therefore the vulnerability to tidal effects is larger.

Figure 15 gives the nondimensional merger rate $R = R(\infty)$ as a function of E_t. The dependence of R_∞ on E_t is similar for different models. For rich clusters with $E_t \sim 0.02$, the merger rate is $\frac{3}{4}$ to $\frac{1}{2}$ of the value for $E_t = 0$. For a

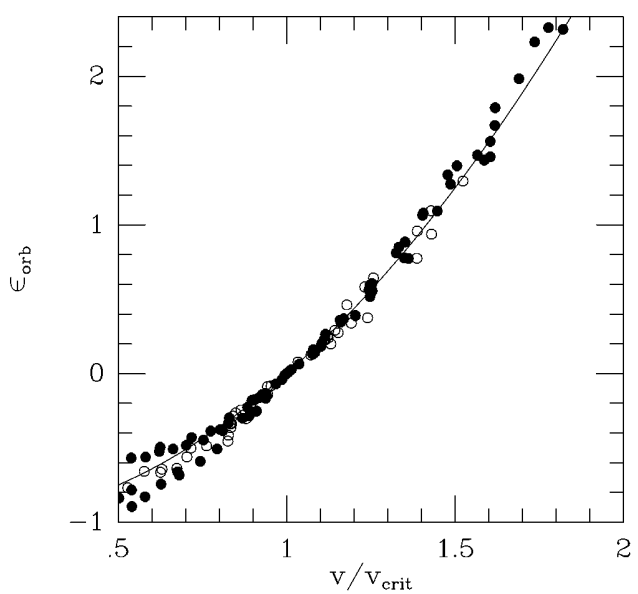

FIG. 13.—Normalized orbital energy $\epsilon_{\rm orb}$ (eq. [52]) after the first encounter plotted against $v/v_{\rm crit}$, the initial relative velocity at infinity in units of the critical velocity for merging. Open circles are the results for the Plummer model, and filled circles are those for the Hernquist model. The curve shows the approximation that ΔE is independent of v (eq. [51]).

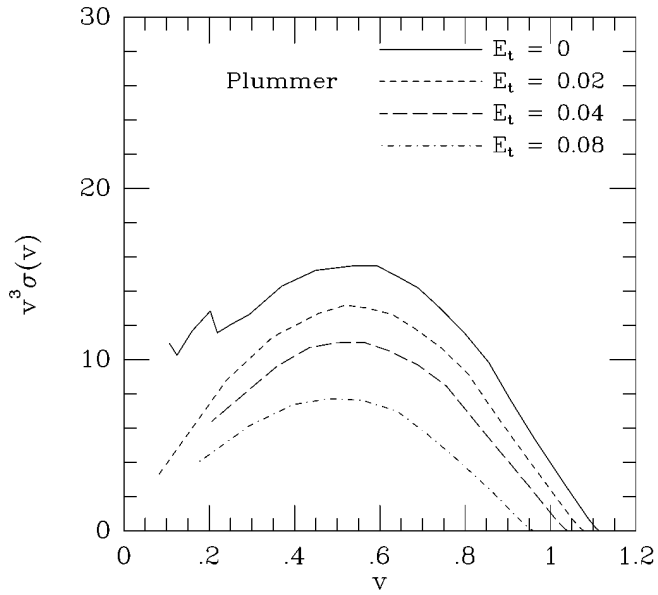

FIG. 14*a*

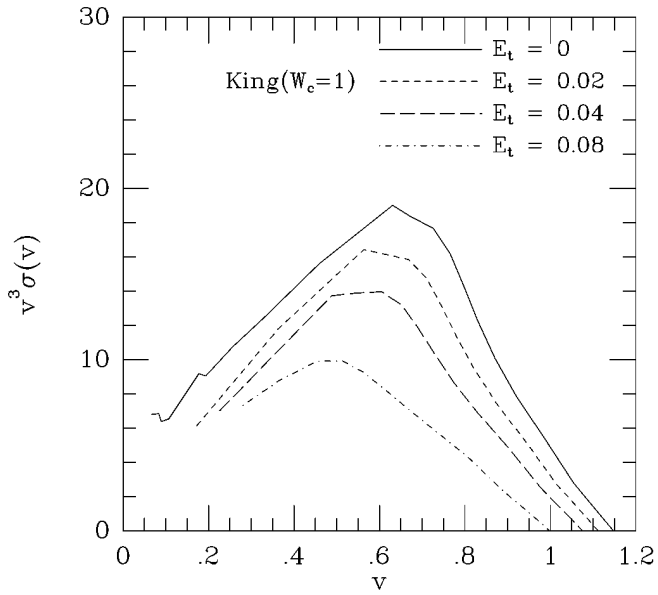

FIG. 14*b*

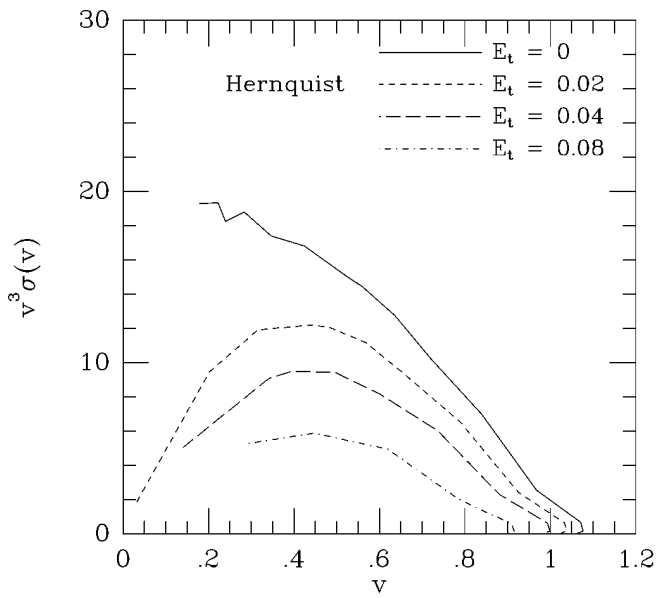

FIG. 14*c*

FIG. 14.—Same as Fig. 9, but for nonzero values of the critical binding energy for tidal disruption E_t. Solid, short-dashed, long-dashed, and dot-dashed curves are results for $E_t = 0, 0.02, 0.04, 0.08$, respectively. (*a*) Plummer, (*b*) King model with $W_c = 1$, (*c*) Hernquist model.

more modest cluster, with $E_t \sim 0.08$, the merger rate has dropped to $\frac{1}{3}$–$\frac{1}{5}$ of the value for $E_t = 0$.

Theoretically, R should reach zero for some finite value of E_t. Thus, a fitting formula of the form

$$R = R_0\left(\frac{E_{t,0} - E_t}{E_{t,0}}\right)^{\gamma} \tag{54}$$

would be an appropriate formula. We found $E_{t,0} = 0.25$ and $\gamma = 3$ to give a reasonable fit for both a King model ($W_c = 7$) and a Plummer model.

6. APPLICATIONS: MERGING IN CLUSTERS OF GALAXIES

As a straightforward application of the merger rates we have determined in the preceding sections, let us take a cluster of galaxies with a three-dimensional spatial density n and a one-dimensional velocity dispersion σ_e for the motion of the galaxies in the cluster. These galaxies are all considered to be given by identical Hernquist models, with half-mass radius r_h and internal one-dimensional velocity dispersion σ_i. We can use the asymptotic expression R_∞ for the merger rate, given by equations (34) and (36), with the relation between the virial radius r_v and the half-mass radius r_h given by equation (4).

For a cluster of galaxies with a one-dimensional velocity dispersion of σ_e km s^{-1}, we can express our main result in physical units as follows. Under the assumption that all galaxies have identical halos, with an internal one-dimensional velocity dispersion of σ_i km s^{-1}, we find a relative merger rate (per unit volume of 1 Mpc^3 Gyr^{-1}) of

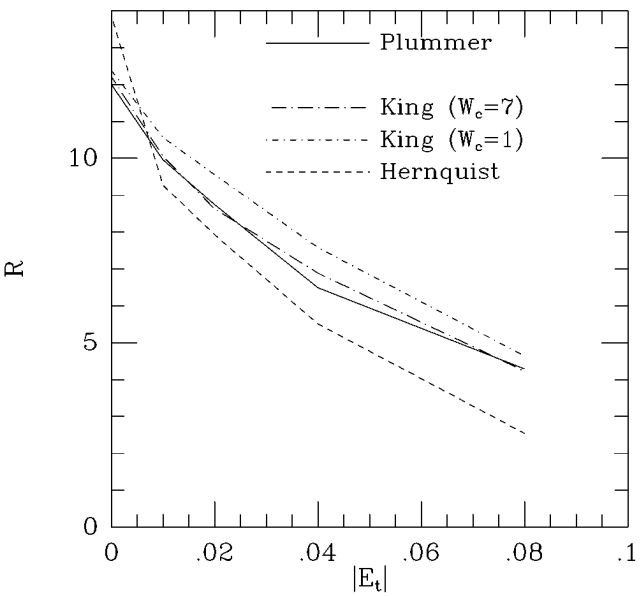

FIG. 15.—Merger rate $R(x)$ as a function of the critical binding energy for tidal disruption E_t. Solid, short–dot-dashed, long–dot-dashed, and short-dashed curves are results for Plummer ($r_{cut} = 23$), King ($W_c = 1$), King ($W_c = 7$), and Hernquist models, respectively.

$$R_{rel} = 0.0084\left(\frac{n}{1\ \mathrm{Mpc}^{-3}}\right)^2\left(\frac{r_h}{0.1\ \mathrm{Mpc}}\right)^2 \times \left(\frac{\sigma_i}{100\ \mathrm{km\ s}^{-1}}\right)^4\left(\frac{300\ \mathrm{km\ s}^{-1}}{\sigma_e}\right)^3 \mathrm{Mpc}^{-3}\ \mathrm{Gyr}^{-1}, \quad (55)$$

where n is the density of galaxies in the galaxy cluster. If we approximate the cluster by a collection of N galaxies evenly distributed within a radius R, we find a total merger rate of

$$R_{tot} = 0.0020N^2\left(\frac{1\ \mathrm{Mpc}}{R}\right)^3\left(\frac{r_h}{0.1\ \mathrm{Mpc}}\right)^2 \times \left(\frac{\sigma_i}{100\ \mathrm{km\ s}^{-1}}\right)^4\left(\frac{300\ \mathrm{km\ s}^{-1}}{\sigma_e}\right)^3 \mathrm{Gyr}^{-1}, \quad (56)$$

corresponding to a fiducial merger timescale of $t_m = 5.0 \times 10^{11}$ yr. In order for merging to occur at a rate that is significant over a Hubble time, we would require a rate that is 2 orders of magnitudes larger. For example, we could take a cluster with 100 galaxies, within a radius of 1 Mpc. If we keep the same fiducial values for the other parameters given in equation (56), mergers would occur at a rate of, on average, once every 50 Myr.

This merger rate is an overestimate, however, since we have not yet taken into account the disruptive effects of tidal interactions, which was discussed in the previous section. The corresponding correction factor, stemming from a finite E_t, is fairly large. For example, for $N = 100$, $D = 10$, and $\sigma_i/\sigma_g = 0.33$, the correction factor R/R_0 is around 0.25. Thus, we conclude that in the above case a merger occurs only once every 200 Myr.

Here we assumed that the cluster is in dynamical equilibrium, which is certainly not true for clusters with, for example, substructures. To apply our result to such clusters, we need rather detailed knowledge about how the substructures evolve.

7. SUMMARY

We have presented cross sections (§ 3) and reaction rates (§ 4) for merging events to occur during encounters of equal-mass spherical galaxies, first in isolation and then in the presence of a background cluster (§ 5). Our results are easily applied to estimate the merger rate in clusters of galaxies (§ 6).

At first glance, the restriction to spherical galaxies might seem somewhat restrictive. However, our numerical calculations as well as our very successful analytic approximations show that the merger rate is largely determined by the outer few-to-10 percent of the mass distribution in the galaxies. For realistic galaxies, even with only a relatively small amount of dark matter, it is therefore the halo mass distribution that determines the merger rate. Even if halos were significantly flattened, it would be rather surprising if our results would be affected by more than a factor of 2. For practical purposes, therefore, we are confident that our results can be applied to galaxy clusters directly as they are given in § 6.

We thank the referee, Josh Barnes, for helpful comments on the manuscript. This work was supported in part by the Grant-in-Aid for Specially Promoted Research (04102002) of the Ministry of Education, Science, and Culture of Japan, by the National Science Foundation under grant PHY89-04035 and under an Advanced Scientific Computing grant ASC-9612029, and by a grant from the Ministry of Education of Japan for a summer visit of P. H. to Kyoto. P. H. acknowledges the hospitality of Dr. Masataka Fukugita and the Yukawa Institute for Theoretical Physics in Kyoto, where this paper was started. We both acknowledge the hospitality of the Institute for Theoretical Physics in Santa Barbara, where we continued to write part of this paper.

REFERENCES

Aarseth, S. J., Hénon, M., & Wielen, R. 1974, A&A, 37, 183
Aguilar, L. A., & White, S. D. M. 1985, ApJ, 295, 374
Barnes, J., & Hernquist, L. 1992, ARA&A, 30, 705
Dekel, A., Lecar, M., & Shaham, J. 1980, ApJ, 241, 946
Heggie, D. C., & Mathieu, R. D. 1986, in The Use of Supercomputers in Stellar Dynamics, ed. P. Hut & S. McMillan (Dordrecht: Springer), 233
Hernquist, L. 1990, ApJ, 356, 359
Makino, J. 1991, PASJ, 43, 859
Okumura, S. K., Makino, J., Ebisuzaki, T., Ito, T., Fukushige, T., Sugimoto, D., Hashimoto, E., Tomida, K., & Miyakawa, N. 1993, PASJ, 45, 329
Richstone, D. O. 1975, ApJ, 200, 535
Richstone, D. O., & Malumuth, E. M. 1983, ApJ, 268, 30
Spitzer, L. 1987, Dynamical Evolution of Globular Clusters (Princeton: Princeton Univ. Press)
Teuben, P. J. 1995, in Astronomical Data Analysis Software and Systems IV, ed. R. Shaw, H. E. Payne, & J. J. E. Hayes (PASP Conf. Ser. 77), 398
White, S. D. M. 1979, ApJ, 229, L9